# Noise in optical synthesis images. II. Sensitivity of an ${}^nC_2$ interferometer with bispectrum imaging

**Shrinivas R. Kulkarni**

*Palomar Observatory 105-24, California Institute of Technology, Pasadena, California 91125*

**Sudhakar Prasad**

*Center for Advanced Studies, University of New Mexico, Albuquerque, New Mexico 87131*

**Tadashi Nakajima**

*Harvard–Smithsonian Center for Astrophysics, 60 Garden Street, Cambridge, Massachusetts 02138*

Received April 9, 1990; accepted September 17, 1990

We study the imaging sensitivity of a ground-based optical array of $n$ apertures in which the beams are combined pairwise, as in radio-interferometric arrays, onto $n(n-1)/2$ detectors, the so-called ${}^nC_2$ interferometer. Ground-based operation forces the use of the fringe power and the bispectrum phasor as the primary observables rather than the simpler and superior observable, the Michelson fringe phasor. At high photon rates we find that bispectral imaging suffers no loss of sensitivity compared with an ideal array (space based) that directly uses the Michelson fringe phasor. In the opposite limit, when the number of photons per spatial coherence area per coherence time drops below unity, the sensitivity of the array drops rapidly relative to an ideal array. In this regime the sensitivity is independent of $n$, and hence it may be efficient to have many smaller arrays, each operating separately and simultaneously.

## 1. INTRODUCTION

The quest for high angular resolution has always been one of the main driving forces in modern astronomy. This is of great importance especially at optical wavelengths since most of the astronomical sources shine in the visible window. Unfortunately, the atmosphere corrupts the light rays coming from cosmic sources, leading to a severe loss in the angular resolution of ground-based observations. In the past few years, new techniques, especially interferometric techniques, have successfully constructed diffraction-limited images of cosmic sources. In view of the many optical interferometers that are either being built or planned we believed it worthwhile to investigate systematically their theoretical performance, particularly in regard to their noise characteristics.

In the first paper of this series[1] we investigated the sensitivity of an ideal Michelson interferometer, which, in the optical domain, is essentially limited by the photoelectron shot noise. A space-based interferometer is a good approximation of an ideal Michelson interferometer. In this paper and another paper[2] we study the theoretical performances of ground-based interferometers.

The principal difference between a space-based and a ground-based interferometer is that the primary observable of the former is the fringe phasor, while the fringe power and the bispectrum phasor are the observables of the latter. While the Michelson fringe phasor is associated with two apertures, the bispectrum or the triple product is the phasor associated with a triplet of apertures. For example, consider three apertures located at $\mathbf{a}_1$, $\mathbf{a}_2$, and $\mathbf{a}_3$. The Michelson fringe phasor $z_{jk}$ is a measure of the cross correlation of the electric field at $\mathbf{a}_j$ and $\mathbf{a}_k$. The bispectrum phasor associated with the three apertures discussed above is $b_{123} \equiv z_{12}z_{23}z_{31}$. According to the van Cittert–Zernike theorem[3] the Michelson fringe phasor $z_{jk}$ is also a measure of the Fourier component of the source structure at the spatial-frequency vector $(\mathbf{a}_j - \mathbf{a}_k)/\lambda$, where $\lambda$ is the mean wavelength of observations. This Fourier relation permits us to determine the brightness distribution of the object, provided that a sufficient number of Fourier components are measured. The van Cittert–Zernike relation is the basis of all interferometric imaging.

Atmospheric turbulence corrupts both the phase and the amplitude of the Michelson fringe phasor. Fortunately, the situation is not totally hopeless. The fringe power after the process of calibration provides a good estimate of the fringe amplitude. The phase of the bispectrum can be shown to be immune to aperture-dependent phase errors. In the parlance of radio astronomy, the phase of the bispectrum is the so-called closure phase,[4] which is the sum of the three Michelson fringe phases and thus contains some information on the spatial structure of the source at the three spatial frequencies. Although there is no direct relation between the bispectrum phasors and the object distribution, astronomers have developed many nonlinear algorithms[4] for constructing images from fringe powers and bispectrum phasors. We refer to this class of algorithms as bispectral-imaging algorithms.

Consider a ground-based optical interferometer consisting of $n$ primary apertures. There are many ways of combining the $n$ primary beams. In Ref. 1 we introduced a useful notation for succinctly describing the beam-combina-

0740-3232/91/030499-12$05.00 

tion geometry. An interferometer in which $r$ beams are combined on one detector is denoted by ${}^nC_r$. This notation has the principal advantage that the number of detectors needed is equal to ${}^nC_r = n!/r!(n-r)!$. In that paper we showed that the sensitivity of an ideal interferometer was essentially independent of the beam-combination geometry. However, the sensitivity of ground-based interferometers, whose primary observables are the bispectrum phasors and the fringe powers, is expected to be dependent on the beam-combination geometry. Understanding this issue is the main goal of this paper. Here we analyze the sensitivity of an ${}^nC_2$ interferometer.

The organization of this paper is as follows. In Section 2 we list the assumptions made and the notation used in our calculations. In Section 3 we evaluate the complete covariance matrix of the two principal observables: the fringe power (from which the fringe amplitude is derived) and the bispectrum phasor (from which the closure phase is derived). We then do a reasonably rigorous calculation of the signal-to-noise ratio (SNR) in the synthesized image and evaluate the SNR of a point source in Section 4. In Section 5 we compare the sensitivity of images obtained from the bispectrum data and those obtained with the self-calibration method (a popular technique at radio wavelengths that also overcomes atmospheric phase errors). We conclude with Section 6.

## 2. ASSUMPTIONS, NOTATION, AND METHODOLOGY

A conventional radio interferometer such as the Very Large Array[5] is a prime example of an ${}^nC_2$ interferometer since the correlators combine signals from pairs of antennas. At optical wavelengths, owing to the lack of low-noise phase-coherent amplifiers, this would require that the primary beam be split $n-1$ ways. Each of these $n(n-1)$ secondary beams can then be correlated pairwise in order to yield $n(n-1)/2$ fringe phasors $z_{jk}$. In turn these fringe phasors can be combined in order to yield $n(n-1)(n-2)/6$ bispectrum phasors $b_{jkl}$. With the use of standard imaging algorithms developed for radio astronomy interferometers,[4] the bispectrum phases in conjunction with the fringe powers can be used to obtain a true image.

We assume that the observations are made with an ideal photon-counting detector with negligible dark current. This condition is met by all modern detectors based on the photoelectric effect. We also assume that there is no significant background radiation.

We further assume that the integration time and the aperture sizes are sufficiently small that there is no significant decorrelation introduced. This is, of course, not strictly true since a real interferometer utilizes finite apertures, a finite bandwidth, and a finite integration time, all of which result in some decorrelation. These aspects are considered in some detail in Ref. 6. In that paper we restrict our attention to the limitations imposed by the photoelectron statistics. These two effects, the decorrelation by the atmosphere and the photoelectron noise, are separable to the first order, and hence the results presented here still have applicability, at least as far as one's understanding of the relative merits of different beam-combination geometries is concerned.

We use the following notation:

$n$ is the number of primary apertures.

$n_b$ is the number of nonzero spatial frequencies offered by an $n$-aperture interferometer, equal to $n(n-1)/2$.

$n_t$ is the number of triangles or bispectrum phasors, equal to $n(n-1)(n-2)/6$.

$z_{jk}$ is the complex fringe phasor on the baseline connecting apertures $j$ and $k$.

$b_{jkl}$ is the bispectrum phasor defined by the apertures $j$, $k$, and $l$, equal to $z_{jk}z_{kl}z_{lj}$.

We will use two notations for indicating baselines and triple products: an aperture-based notation and a baseline-based notation. In the first scheme $z_{jk}$ is the fringe phasor on the baseline defined by apertures $j$ and $k$. In the second scheme a single index is used, ranging from 1 to $n_b$. A corresponding scheme is used for the bispectrum phasors. The disadvantage of these schemes is that the notation for the bispectrum phasor is formally the same for both schemes and can lead to confusion unless clarified. In addition, in the baseline-based scheme, the indexing is quite arbitrary in the sense that a baseline index $j$ does not uniquely specify a particular baseline (see Fig. 1 for an example of this indexing scheme). In recognition of this problem we clarify both the kind of notation used and the indexing scheme, when necessary.

We will use lowercase letters for observables derived from a single frame of data and the corresponding uppercase letters for the mean values of those observables. For example, $z_j$ is the fringe phasor from baseline $j$ obtained from one frame of data, whereas $Z_j$ is the ensemble average or the mean of $z_j$ averaged across many frames.

We use the symbol $V$ to denote the variance of a real observable (say $x$), $V(x) = \langle x^2\rangle - \langle x\rangle^2$, and the pseudovar-

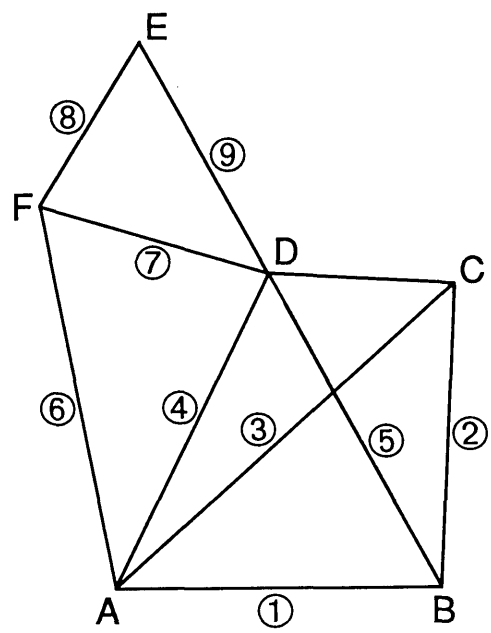


Fig. 1. Baseline-based indexing scheme for the bispectrum phasor for a six-element array. The baseline connecting apertures A and B is assigned the index 1, that connecting B and C the index 2, etc. Not all the baselines are shown.

iance of a complex observable such as the fringe phasor $V(z) \equiv \langle zz^* \rangle - \langle z \rangle \langle z^* \rangle$. The covariance of a pair of real observables $x$ and $y$ is specified by $C(x, y) = \langle xy \rangle - \langle x \rangle \langle y \rangle$. For pairs of complex observables $z_1$ and $z_2$, there are two kinds of covariance:

(1) Pairs of unconjugated quantities, $C(z_1, z_2) = \langle z_1 \rangle \langle z_2 \rangle$.
(2) Pairs of conjugated quantities, $C(z_1, z_2^*) = \langle z_1 z_2^* \rangle - \langle z_1 \rangle \langle z_2^* \rangle$.

We evaluate both types of covariance and note that what is usually needed is the sum of these two quantities, which we refer to as the pseudocovariance.

Unlike an ideal Michelson interferometer for which we have the van Cittert–Zernike relation, there is no equivalent linear relation between the bispectrum phasor and the image. The bispectral-imaging algorithms are iterative, and hence a simple error analysis is, in general, not possible. Fortunately, for the simple but important case of a point source, there is a simple relationship between the observables and the image. This permits us to estimate the variance in the synthesized image, given the covariance matrix of the bispectrum phasor. Such a procedure was followed in Ref. 1, and we follow a similar strategy here.

## 3. $^nC_2$ INTERFEROMETERS

As stated in Section 1, each of the $n$ primary beams is divided into $n - 1$ secondary beams. The $n(n - 1)$ secondary beams are combined pairwise, yielding $n_b = n(n - 1)/2$ fringes. The intensity pattern on any of the $n_b$ detectors is of the form

$$I_j(x) = 2I_0\left[1 + \gamma_j \cos\left(2\pi \frac{B_i}{\lambda}\frac{x}{d} + \phi_j + \theta_j\right)\right], \tag{3.1}$$

where $\gamma_j \exp i\phi_j$ is the complex visibility function (or the complex spatial-coherence function), $B_j$ is the baseline connecting a pair of apertures, $\lambda$ is the mean wavelength of the light, $d$ is the distance between the aperture and detector planes, $x$ is the coordinate in the aperture plane, and $\theta_j$ is the phase imposed by the irregularities in the atmosphere; here $j$ is the index of the baseline and can range from 1 to $n_b$. Let $k_j(p)$ be the number of photoelectrons per integration interval at pixel $p$ of detector of baseline $j$. We assume that the detector is a linear array of $P$ pixels. The corresponding mean photoelectric count distribution is given by

$$\langle k_j(p) \rangle = 2\langle K \rangle [1 + \cos(p\omega_j + \phi_j + \theta_j)]. \tag{3.2}$$

Here $2\langle K \rangle$ is proportional to the mean incident intensity and $\omega_j$ is proportional to the spatial frequency (and absorbs $\lambda$, pixel spacing, etc.). The estimator for the complex visibility function is the fringe phasor defined in the usual way:

$$z_j = \sum_{p=0}^{P-1} k_j(p)\exp(-i\omega_j p). \tag{3.3}$$

The mean number of photoelectrons per detector is $2\langle K \rangle P$, and thus the average number of photoelectrons from each secondary beam is $\langle N \rangle = \langle K \rangle P$.

Imaging requires both amplitude and phase information. As clarified in Section 1, atmospheric irregularities corrupt the Michelson phase, forcing us to use closure phases (i.e., bispectrum phasors). Likewise, we are forced to use the fringe power as an estimator of the fringe amplitude. (The modulus of the fringe phasor $|z_{jk}|$ can also be used as an estimator of the fringe amplitude. However, the noise properties of the fringe power are easily calculable, and there is no extra gain in the SNR by using the modulus of the fringe phasor instead of the fringe power.) We now estimate the covariance properties of both these observables.

### A. Variance and Covariance of Fringe Power

The fringe power

$$p_j = z_j z_j^* \tag{3.4}$$

is uncorrupted by the atmospheric phase perturbations and hence is a good observable. In reality, significant and systematic decorrelation by the atmosphere does take place, but this is expected to be removed by the process of calibration. Further discussion of this issue appears in Ref. 6.

The mean value of $p_j$ is

$$P_j = \left\langle \sum_{p=0}^{P-1} \exp(-i\omega_j p)k_j(p) \sum_{p=0}^{P-1} \exp(i\omega_j p')k_j(p') \right\rangle. \tag{3.5a}$$

Since $\langle k_j(p)k_j(p') \rangle = \langle k_j(p) \rangle \langle k_j(p') \rangle + \delta_{pp'} \langle k_j(p) \rangle$, we obtain

$$P_j = Z_j Z_j^* + \sum_{p=0}^{P-1} \langle k_j(p) \rangle$$
$$= \gamma_j^2 \langle N \rangle^2 + 2\langle N \rangle. \tag{3.5b}$$

Here $\gamma_j$ is the normalized fringe visibility. From Eq. (3.5b) it is clear that $p_j$ is biased; i.e., $P_j \neq 0$ even when $\gamma_j = 0$. This happens since the information of the classical fringe power is contained only in the cross correlations of different photoelectron events. This bias can be eliminated[7] by its subtraction,

$$q_j = p_j - \sum_{p=0}^{P-1} k_j(p), \tag{3.6}$$

the mean of which is

$$Q_j \equiv \langle q_j \rangle = \gamma_j^2 \langle N \rangle^2. \tag{3.7}$$

The derivation of the variance of the fringe power $q_j$ is straightforward but somewhat cumbersome owing to the bias correction. This can be shown to be (see Appendix A)

$$V(q_j) = 4\langle N \rangle^2 (1 + \gamma_j^2 \langle N \rangle). \tag{3.8a}$$

The SNR of $q_j$, i.e., the ratio of $Q_j$ to $[V(q_j)]^{1/2}$, is

$$\mathcal{S}_{Q_j} = \frac{\gamma_j^2 \langle N \rangle}{2(1 + \gamma_j^2 \langle N \rangle)^{1/2}}. \tag{3.8b}$$

The asymptotic behavior of $\mathcal{S}_{Q_j}$ is quite interesting: For the high photoelectron rate ($\gamma_j^2 \langle N \rangle \gg 1$), $\mathcal{S}_{Q_j} \sim (\gamma_j/2)\sqrt{\langle N \rangle}$. For the low photoelectron rate ($\gamma_j^2 \langle N \rangle \ll 1$), $\mathcal{S}_{Q_j} \sim \gamma_j^2 \langle N \rangle /2$. The transition from the low photoelectron rate to the high photoelectron rate occurs at $\gamma_j^2 \langle N \rangle \sim 1$.

We next evaluate the covariance of pairs of fringe powers. Consider the covariance between $q_j$ and $q_k^* (j \neq k)$:

$$
\begin{aligned}
C(q_j, q_k^*) &= \langle q_j q_k^* \rangle - \langle q_j \rangle \langle q_k^* \rangle \\
&= \sum_{pp'} \sum_{rr'} \langle [k_j(p)k_j(p') - \delta_{pp'}\langle k_j(p)\rangle][k_k(r)k_k(r') \\
&\quad - \delta_{rr'}\langle k_k(r)\rangle]\rangle \exp[-i\omega_j(p-p')]\exp[-i\omega_k(r'-r)] \\
&\quad - Q_j Q_k^* \\
&= 0.
\end{aligned}
\tag{3.9}
$$

The lack of statistical correlation between any two different fringe phasors is obviously a result of the physical independence of the detectors.

### B. Pseudovariance and Covariance of the Bispectrum

The bispectrum, or the triple product $b_{jkl}$, is defined to be the product of three fringe phasors on baselines that form a triangle. For example, for Fig. 1 the triangle formed by baselines 1, 2, and 3 defines the bispectrum phasor:

$$
b_{123} = z_1 z_2 z_3. \tag{3.10}
$$

Throughout this section, unless otherwise stated, we use the baseline-based indexing scheme (Section 2).

When the baselines $j$, $k$, and $l$ close, i.e., when they form a true triangle, then the atmospheric terms cancel and the phase of $b_{jkl}$ is given by $\psi_{jkl} = \phi_j + \phi_k + \phi_l$, a sum of pure source structure phases. Because of its immunity to the atmospheric corruption, the bispectrum can be added across integrations in order to yield a mean bispectrum phasor:

$$
\begin{aligned}
B_{jkl} &= \langle b_{jkl} \rangle \\
&= \left\langle \sum_{p=0}^{P-1} k_j(p)\exp(-i\omega_j p) \sum_{q=0}^{P-1} k_k(q) \right. \\
&\quad \left. \times \exp(-i\omega_k q) \sum_{r=0}^{P-1} k_l(r)\exp(-i\omega_l r) \right\rangle \\
&= \sum_{pqr} \exp(-i\omega_j p - i\omega_k q - i\omega_l r)\langle k_j(p)k_k(q)k_l(r)\rangle.
\end{aligned}
\tag{3.11}
$$

As clarified in Section 2, the averaging procedure $\langle \cdots \rangle$ is assumed to include only the statistics of the photoelectron process and not any decorrelation introduced by the atmosphere. (Even in the absence of atmosphere-introduced phase and intensity fluctuations, there will be additional intensity fluctuations owing to the thermal nature of the astronomical signal. This effect is completely negligible for astronomical sources because of the low signal strengths.)

Since the detectors are separate, the photoelectric-detection noise does not correlate. Thus

$$
\langle k_j(p)k_k(q)k_l(r)\rangle = \langle k_j(p)\rangle\langle k_k(q)\rangle\langle k_l(r)\rangle. \tag{3.12}
$$

We therefore find that

$$
\begin{aligned}
B_{jkl} &= Z_j Z_k Z_l \\
&= \gamma_j \gamma_k \gamma_l \langle N\rangle^3 \exp(-i\psi_{jkl}).
\end{aligned}
\tag{3.13}
$$

Note that $B_{123}$, unlike the fringe power, is not biased. The absence of bias here is in contrast with the situation when all the $n$ beams interfere on the same detector.[8] In the latter case the bias arises since a given photoelectron cannot be ascribed uniquely to one of the $n_b$ fringe patterns. In an ${}^nC_2$ interferometer the fringe patterns are separately detected, and thus the fringe phasors are statistically independent, which explains the absence of the bias. This discussion also highlights one of the virtues of an ${}^nC_2$ interferometer, viz., the simplicity in modeling the observables and their noise distribution. This is an important advantage since it permits one to estimate *ab initio* the SNR in the synthesized image, and thus the interpretation of faint features in the synthesized image is quite straightforward.

We note that, in contrast to that for an ${}^nC_2$ interferometer, the estimation of the noise distribution in a ${}^nC_n$ interferometer is exceedingly difficult. First, the expression for the variance of the bispectrum phasor[9,10] is quite involved. The noise distribution in the image is naturally even more complicated, and further discussion of this issue is found in Ref. 2.

Specifically, we will consider one particular bispectrum $b_{123}$. The pseudovariance of $b_{123}$ is easily estimated:

$$
\begin{aligned}
V(b_{123}) &\equiv \langle b_{123} b_{123}^* \rangle - \langle b_{123} \rangle \langle b_{123}^* \rangle \\
&= \langle z_1 z_2 z_3 z_1^* z_2^* z_3^* \rangle - \langle z_1 z_2 z_3 \rangle \langle z_1^* z_2^* z_3^* \rangle.
\end{aligned}
\tag{3.14}
$$

The detectors' being separate permits us to rewrite Eq. (3.14) as

$$
V(b_{123}) = \langle z_1 z_1^* \rangle \langle z_2 z_2^* \rangle \langle z_3 z_3^* \rangle - \gamma_1^2 \gamma_2^2 \gamma_3^2 \langle N\rangle^6. \tag{3.15}
$$

Substituting Eq. (3.5) into Eq. (3.15), we find that

$$
\begin{aligned}
V(b_{123}) &= 2\langle N\rangle^5(\gamma_1^2\gamma_2^2 + \gamma_2^2\gamma_3^2 + \gamma_3^2\gamma_1^2) \\
&\quad + 4\langle N\rangle^4(\gamma_1^2 + \gamma_2^2 + \gamma_3^2) + 8\langle N\rangle^3.
\end{aligned}
\tag{3.16}
$$

The SNR, $\mathcal{S}_{B_{123}} \equiv |B_{123}|/[V(b_{123})]^{1/2}$ of the bispectrum is

$$
\mathcal{S}_{B_{123}} = \frac{\gamma_1\gamma_2\gamma_3\langle N\rangle^{3/2}}{[2\langle N\rangle^2(\gamma_1^2\gamma_2^2 + \gamma_2^2\gamma_3^2 + \gamma_3^2\gamma_1^2) + 4\langle N\rangle(\gamma_1^2 + \gamma_2^2 + \gamma_3^2) + 8]^{1/2}}. \tag{3.17}
$$

We now investigate the covariance between pairs of bispectrum phasors. For specificity we consider one of the phasors to be $b_{123}$:

$$
C(b_{123}, b_{jkl}^*) = \langle b_{123} b_{jkl}^* \rangle - \langle b_{123} \rangle \langle b_{jkl}^* \rangle. \tag{3.18}
$$

We remind the reader that the baselines $jkl$ must form a triangle and cannot be any three arbitrary baselines.

The triangle defined by the indx $jkl$ can fall into any one of only three categories (see Fig. 1):

(1) Triangle $jkl$ does not share a common aperture with triangle 123, e.g., triangle 789.

(2) Triangle $jkl$ shares a common primary aperture with triangle 123, e.g., triangle 467.

(3) Triangle $jkl$ shares a common baseline, e.g., triangle 145.

Bispectrum phasors of triangles of the first kind follow independent statistics since they do not share any common fringe phasor at all. Thus the covariance of such bispectrum phasors with $b_{123}$ is zero. Essentially the same arguments apply to triangles that share a common primary aperture.

Thus one need consider only triangles with one side in common with triangle 123, e.g., triangle 145, for which we find that

$$\begin{aligned} C(b_{123}, b_{145}^*) &= \langle z_1 z_1^* \rangle \langle z_2 \rangle \langle z_3 \rangle \langle z_4^* \rangle \langle z_5^* \rangle \\ &\qquad - \langle z_1 \rangle \langle z_2 \rangle \langle z_3 \rangle \langle z_1^* \rangle \langle z_4^* \rangle \langle z_5^* \rangle \\ &= [\langle z_1 z_1^* \rangle - \langle z_1 \rangle \langle z_1^* \rangle] \langle z_2 \rangle \langle z_3 \rangle \langle z_4^* \rangle \langle z_5^* \rangle \\ &= 2\gamma_2\gamma_3\gamma_4\gamma_5 \langle N \rangle^5 \exp(i\psi_{123} - i\psi_{145}). \end{aligned} \tag{3.19}$$

We also need to estimate the covariance of unconjugated pairs of bispectrum phasors with one common side, e.g., 123 and 145:

$$\begin{aligned} C(b_{123}, b_{145}) &= \langle z_1 z_2 z_3 z_1 z_4 z_5 \rangle - \langle z_1 z_2 z_3 \rangle \langle z_1 z_4 z_5 \rangle \\ &= (\langle z_1 z_1 \rangle - \langle z_1 \rangle \langle z_1 \rangle) \langle z_2 \rangle \langle z_3 \rangle \langle z_4 \rangle \langle z_5 \rangle \\ &= \left\langle \sum_p k(p) \exp(-i2\omega_1 p) \right\rangle \gamma_2\gamma_3\gamma_4\gamma_5 \\ &\quad \times \exp(i\psi_{123} + i\psi_{145}) \\ &= 0. \end{aligned} \tag{3.20}$$

The sum of both these types of covariance $C(b_{123}, b_{145}) + C(b_{123}, b_{145}^*)$ is of some interest [see the discussion following Eq. (4.2)]; we call this quantity pseudocovariance. A related quantity is the normalized covariance element $\mu_{123,145}$, which is defined as the ratio of the pseudocovariance to the geometric mean of the individual pseudovariances:

$$\mu_{123,145} \equiv \frac{C(b_{123}, b_{145}) + C(b_{123}, b_{145}^*)}{[V(b_{123}) V(b_{145})]^{1/2}}. \tag{3.21}$$

Note that $\mu_{123,145}$ is insensitive to the relative orientation of the common baseline between the two triangles. Here we considered the case when the common side had the same orientation in both triangles. For those pairs of triangles for which the common side is oriented oppositely, Eq. (3.19) will yield zero, but Eq. (3.20) will not. The sum [Eq. (3.21)] is thus unaffected.

So far the discussion has been quite general. Consider for simplicity the case when all the visibilities are equal ($\gamma_j = \gamma$, independent of $j$), and all the closure phases are zero. Then

$$\begin{aligned} B &\equiv B_{jkl} = \gamma^3 \langle N \rangle^3, \\ \sigma_b^2 &\equiv V(b) \equiv V(b_{123}) = \langle N \rangle^3 (6\gamma^4 \langle N \rangle^2 + 12\gamma^2 \langle N \rangle + 8), \\ \mathcal{S}_B &\equiv \frac{B}{\sqrt{V(b)}} = \frac{(\gamma^2 \langle N \rangle)^{3/2}}{(6\gamma^4 \langle N \rangle^2 + 12\gamma^2 \langle N \rangle + 8)^{1/2}}, \\ \mu_b &\equiv \mu_{123,145} = \frac{\gamma^4 \langle N \rangle^2}{3\gamma^4 \langle N \rangle^2 + 6\gamma^2 \langle N \rangle + 4}. \end{aligned} \tag{3.22}$$

Note that $\mathcal{S}_B$ and $\mu_b$ are functions purely of $\gamma^2\langle N \rangle$. Thus the transition from one asymptotic limit to another depends on this combination of $\langle N \rangle$ and $\gamma$:

*High Photoelectron Rate*

At high photoelectron rates ($\gamma^2\langle N \rangle \gg 1$) the pseudovariance is $\sim 6\gamma^4\langle N \rangle^5$, and the SNR of the bispectrum phasors is $\gamma(\langle N \rangle/6)^{1/2}$. In contrast the SNR of the fringe amplitude as measured by an ideal Michelson interferometer[1,11] is $\gamma\sqrt{(2N)}$, which is a factor of $\sqrt{3}$ better. This difference is readily understood as arising from the multiplication of three estimators with identical noise distributions.

In this limit the normalized covariance $\mu_b$ approaches 1/3, independent of $\gamma$. This is quite easy to understand since that is precisely the amount of information shared by the two bispectrum phasors with one common baseline.

*Low Photoelectron Rates*

The low photoelectron rate regime ($\gamma^2\langle N \rangle \ll 1$) could be due either to low photoelectron rate $\langle N \rangle \ll 1$) or to a very low normalized fringe visibility ($\gamma \ll 1$). In this regime the SNR of the bispectrum $\mathcal{S}_{b_{123}} \sim \gamma^3\langle N \rangle^{3/2}/\sqrt{8}$. This cubic dependence on $\langle N \rangle$ is quite readily understood and can be argued from physical considerations. First, we estimate the pseudovariance of the bispectrum phasor. At low photoelectron rates, the probability of obtaining a photoelectron on a given detector in one integration time or frame is $\langle N \rangle$; note that is independent of $\gamma$. Only those integration intervals during which at least one photoelectron is detected in each of the three detectors, 1, 2, and 3, are useful for measuring the bispectrum $b_{123}$. The joint probability of such an occurrence is thus $\langle N \rangle^3$. With $m$ frames we expect to obtain an estimate of the closure phasor in only $m\langle N \rangle^3$ frames. Thus the pseudovariance of the bispectrum phasor is $m\langle N \rangle^3$ and the pseudovariance per frame is $\langle N \rangle^3$. The amplitude of the fringe phasor is $\gamma\sqrt{\langle N \rangle}$, regardless of the photoelectron rate. Hence the bispectrum amplitude is $\gamma^3\langle N \rangle^3$. The SNR per frame or integration interval is thus proportional to $\gamma^3\langle N \rangle^{3/2}$, in accordance with our asymptotic formula.

The above physical reasoning also gives insight into why the bispectrum phasor becomes increasingly noisy as $\langle N \rangle$ becomes small, viz., primarily because the fraction of useful frames $\langle N \rangle^3$ becomes small. Also note that the SNR depends cubically on $\gamma$ at low-light levels whereas at high-light levels the SNR is linearly related to $\gamma$. This makes it important to avoid any kind of instrumental decorrelation and also shows that the SNR of the bispectrum decreases dramatically when the source starts getting resolved.

In this regime the normalized correlation coefficient for a pair of bispectrum phasors that share a common phasor is $\sim(1/4)\gamma^4\langle N \rangle^2$. The quadratic dependence of $\mu_b$ on $\langle N \rangle$ can also be physically reasoned out. Above we showed that the pseudovariance of the bispectrum per integration interval is $\langle N \rangle^3$. We now estimate the covariance between $b_{123}$ and $b_{145}$. In order that there be some covariance or cross talk between these bispectrum phasors, both $b_{123}$ and $b_{145}$ need to be detected within the same integration interval, i.e., at least one photoelectron in each of the five detectors, 1–5, must be detected within one integration time. The fringe phasor amplitude in each of the five baselines is $\gamma\langle N \rangle$. The cross talk is thus expected to be $\gamma^5\langle N \rangle^5$; however, the shared baseline is perfectly correlated (i.e., $\gamma = 1$), and thus the cross talk amplitude is $\gamma^4\langle N \rangle^5$. Normalizing this by the pseudovariance of the bispectrum phasor $\langle N\rangle^3$, we find that $\mu_b \sim \gamma^4\langle N\rangle^2$.

The steep dependence of $\mu_b$ on $\langle N\rangle$ or $\gamma$ means that the bispectrum phasors become essentially decorrelated either for faint sources or when the source gets resolved. Thus analysis such as mapmaking should use all the bispectrum phasors, but one should keep in mind the covariance properties of the bispectrum phasors.

In conclusion, the bispectrum phasor becomes rapidly noisy once the quantity $\gamma^2\langle N\rangle$ falls below unity. This is not surprising since the bispectrum is a sixth-order estimator (in electric field), unlike the Michelson fringe phasor, which is a second-order estimator. However, since integrations across a large number of frames can be performed, this noisiness can be partially compensated for.

## 4. SIGNAL-TO-NOISE RATIO IN THE SYNTHESIZED IMAGE

In this section we estimate the pseudovariance and therefore the SNR in the synthesized image. The SNR's of the observables $B_{jkl}$ and $Q_j$ are important from a practical viewpoint. However, as emphasized in Section 1, what ultimately matters is the SNR in the map. Here we estimate the SNR in a map of the simplest source, a point source.

From the discussions in Subsections 3.A and 3.B, it is clear that mapmaking is limited mainly by the SNR of the bispectrum phasor and not by the SNR of the fringe power. This is certainly true at the low light levels. At high light levels the SNR in the bispectrum phasor is linearly related to that of the fringe power. Thus in either limit it is sufficient to consider the SNR of the bispectrum.

For simplicity we consider the specific case of a point source at the phase center for which $\psi_{jkl} = 0$ and $\gamma_j = 1$. This simplification permits us to model the noise in the image plane effectively.

The usual strategy of bispectral imaging algorithms is to make a map based on the $n_b$ mean fringe powers and the $n_t$ closure phases. Since the techniques are iterative there is, in general, no closed-form expression for the synthesized image in terms of the observables. Fortunately, for the simple case of a point source at the phase center, we have a closed-form expression for the only unknown quantity, viz., the flux density of the source. We now estimate the SNR of this quantity and argue that it is a fair measure of the SNR (but is subject to the warnings and caveats discussed below) in the synthesized image.

Consider the vector sum of all the bispectrum phasors

$$F = \langle f\rangle = \sum_{s=1}^{n_t} B_s. \tag{4.1}$$

Here the index $s = 1$ refers to the triangle 123, etc. We argue that $[\mathrm{Re}(F)]^{1/3}$ is a good, if not an optimal, estimator of the flux density of the point source. Noting that $\mathrm{Re}(F) = 1/2(F + F^*)$ we find that the pseudovariance of $\mathrm{Re}(f)$ is

$$\begin{aligned} V[\mathrm{Re}(f)] &= \frac{1}{4}\sum_{s=1}^{n_t}\sum_{t=1}^{n_t} C(B_s, B_t) + C(B_s, B_t^*) \\ &\quad + C(B_s^*, B_t) + C(B_s^*, B_t^*) \\ &= \frac{1}{2}\sum_s\sum_t \mathrm{Re}[\mu_b(s,t)]\sigma_b(s)\sigma_b(t). \end{aligned} \tag{4.2}$$

Equation (3.21) has been used for simplifying the above equation. The quantity $\mu_b(s, t)$ is the normalized pseudocovariance coefficient of the bispectrum phasors $b_s$ and $b_t^*$, and $\sigma_b(s) \equiv [V(b_s)]^{1/2}$ is the standard deviation of the bispectrum phasor $b_s$ (Subsection 3.B). The SNR of the measured flux density is $S/\sigma_S$ and is three times the SNR of $\mathrm{Re}(f)$:

$$\begin{aligned} \frac{S}{\sigma_S} &= \frac{3\mathrm{Re}(F)}{\{V[\mathrm{Re}(f)]\}^{1/2}} \\ &= 3\mathcal{S}_F. \end{aligned} \tag{4.3}$$

The covariance matrix, consisting of $n_t \times n_t$ elements, can be divided into three groups:

(1) Diagonal elements are $n_t$ elements that are the pseudovariances of the closure phasors and are specified by Eq. (3.16).

(2) Nondiagonal elements measure the covariance between a pair of triangles with one common side. The value of these elements is specified by Eq. (3.19). For any given triangle, there are $3(n - 3)$ triangles that have one side in common with the given triangle. Thus the total number of covariance elements of the second kind is $3(n - 3)n_t$.

(3) Nondiagonal elements that measure the covariance between a pair of triangles with no common sides. From the discussion in Subsection 3.B, the value of these elements is zero.

The total variance in $F$ is thus the sum of all the elements in the covariance matrix and is

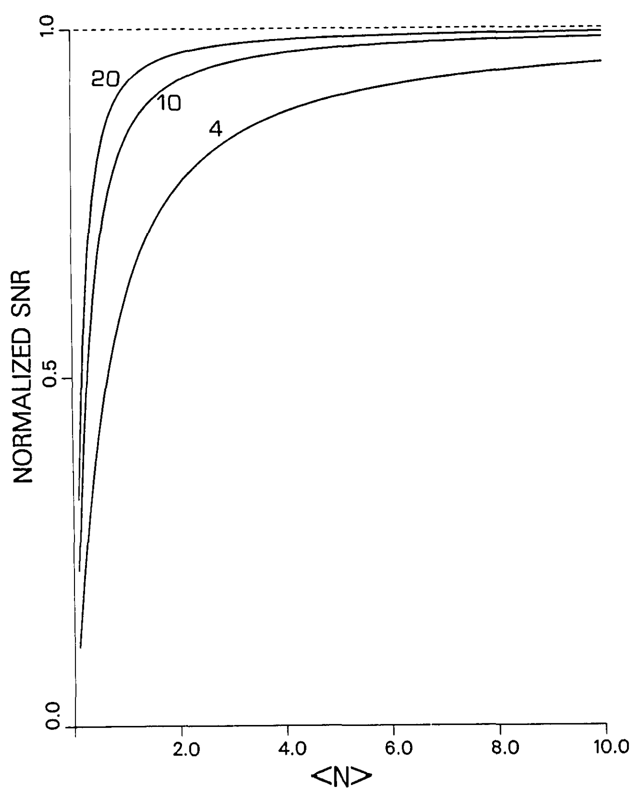


Fig. 2. Ratio of the image SNR for the bispectrum case to that for the ideal case as a function of the photon number $\langle N\rangle$ per subbeam per frame for various values of the number $n$ of apertures. The dashed line represents the ideal case.

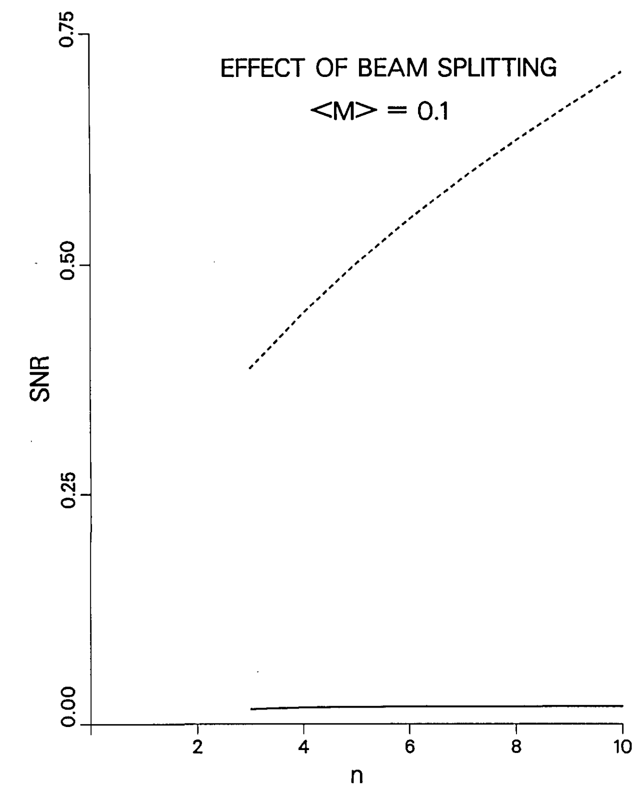


Fig. 3. Image SNR for the bispectrum case as a function of the number $n$ of apertures for a fixed source intensity $\langle M \rangle = 0.1$. $\langle M \rangle$ is the number of photoelectrons per primary aperture per integration time. The dashed curve represents the ideal case.

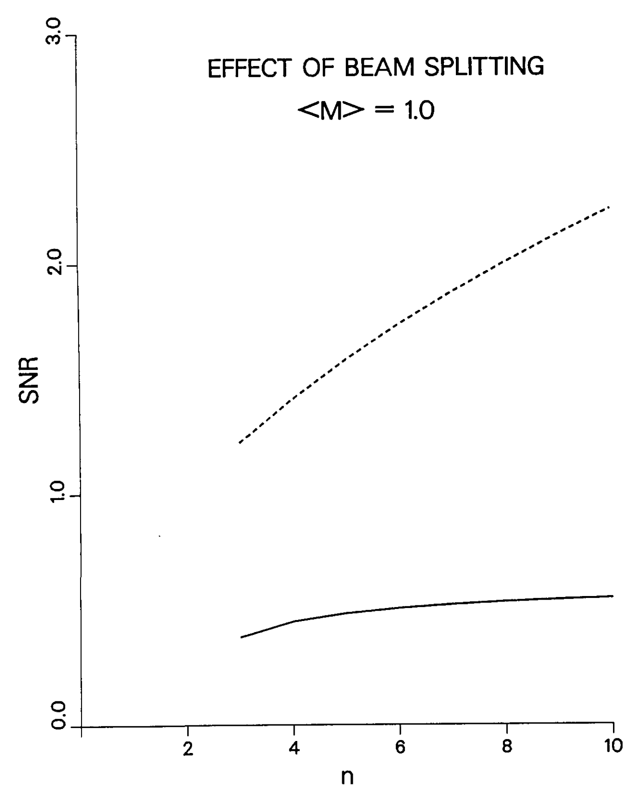


Fig. 4. Same as Fig. 3 but with $\langle M \rangle = 1.0$.

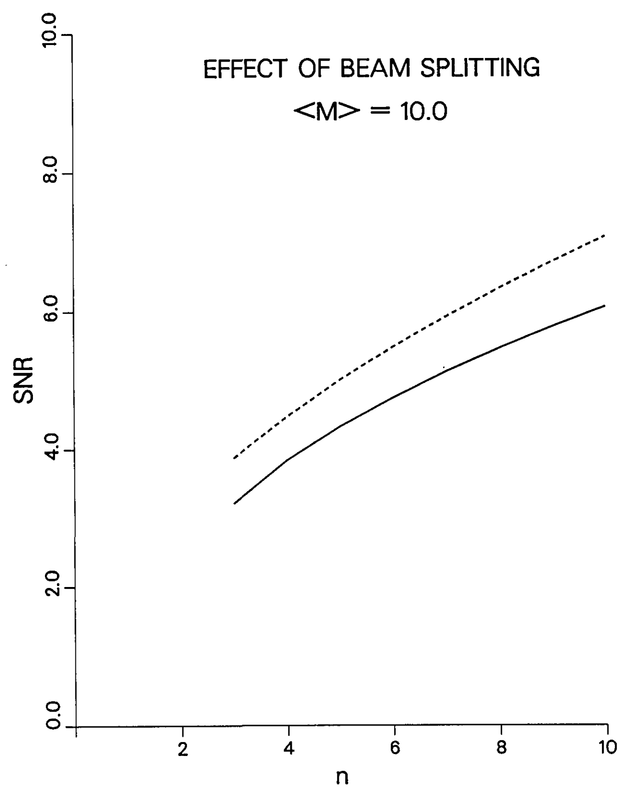


Fig. 5. Same as Fig. 3 but with $\langle M \rangle = 10.0$.

$$V[\mathrm{Re}(f)] = \frac{1}{2}\, n_t \sigma_b{}^2 + \frac{3}{2}\,(n-3) n_t \mu_b \sigma_b{}^2. \tag{4.4a}$$

In Eq. (4.4a) we assume that $\sigma_b{}^2$ and $\mu_b$ are independent of the triangle indices $s$ and $t$. This is certainly true for a point source. In the general case, $\sigma_b{}^2$ and $\mu_b$ are to be interpreted as average values:

$$\mathcal{S}_F = \left[\frac{2n_t}{\sigma_b{}^2 + 3(n-3)\mu_b\sigma_b{}^2}\right]^{1/2} \gamma^3 \langle N \rangle^3. \tag{4.4b}$$

Substituting expressions for $\sigma_b$ and $\mu_b$ from Eqs. (3.22) into Eq. (4.4) and using Eq. (4.3) yield the following result for the SNR of the source flux density:

$$\frac{S}{\sigma_S} = \frac{3\sqrt{n_t}\,\gamma^3 \langle N \rangle^{3/2}}{[3(n-2)\gamma^4\langle N \rangle^2 + 6\gamma^2\langle N \rangle + 4]^{1/2}}. \tag{4.5a}$$

Equation (4.5a) can be rewritten as

$$\frac{S}{\sigma_S} = \frac{\gamma(\langle L \rangle/2)}{\{1 + [(6\gamma^2\langle N \rangle + 4)/3(n-2)\gamma^4\langle N \rangle^2]\}^{1/2}} \tag{4.5b}$$

in terms of $\langle L \rangle = n(n-1)\langle N \rangle$, the mean number of photoelectrons intercepted by the entire $n$-aperture array in one integration interval. Because of the presence of the second term in the denominator of Eq. (4.5b), the SNR is always smaller than $\gamma(\langle L \rangle/2)^{1/2}$, which is the SNR obtained under the ideal conditions of the ${}^nC_2$ Michelson interferometer.[1]

Since the SNR depends on $\gamma$ and $\langle N \rangle$ only through the product $\gamma^2\langle N \rangle$, we will assume for the purposes of graphical illustration that $\gamma$ is unity. In Fig. 2 we have plotted the normalized SNR in the image as a function of $\langle N \rangle$ for various values of $n$, the number of apertures. The SNR has been normalized relative to the ideal value $(\langle L\rangle/2)^{1/2}$, which is designated by a dashed line at unit height. Clearly as the number of apertures increases, the SNR approaches the ideal case faster as a function of $\langle N\rangle$, in accordance with Eqs. (4.5).

The inferiority of the bispectrum phasor as an estimator of the fringe visibility as compared with the Michelson phasor is clearly seen in Figs. 3–5, in which we plot the SNR's for the bispectrum imaging and the ideal imaging as a function of the number $n$ of apertures for a given source strength. The three figures refer to source strengths (given here in terms of the average number $\langle M\rangle$ of photoelectrons arriving at each aperture during an integration interval) equal to 0.1, 1.0, and 10.0. For comparison the ideal case is plotted as a dashed curve on each figure. Clearly as the number of apertures increases, the SNR of bispectrum imaging, low to begin with, falls rapidly further below the ideal case owing to the deleterious effects of beam splitting in the former. This is of course most dramatic at the lowest signal strengths (Fig. 3). The situation is improved by a factor of 2 when no beam splitting is done as in an ${}^nC_n$ array,[2] but the vast inferiority of the bispectrum as the visibility estimator is still quite evident at low signal strengths.

We now consider the SNR in the usual asymptotic limits. From the preceding expression, it is clear that the two limits correspond to whether $\gamma^2\langle N\rangle(n-2)^{1/2}$ is much greater than or much smaller than 1.

### A. High Photoelectron Limit

For the high photoelectron limit $[\gamma^2\langle N\rangle(n-2)^{1/2} \gg 1]$

$$\mathcal{S}_F = \left[\frac{n(n-1)}{18}\right]^{1/2} \gamma\sqrt{\langle N\rangle}. \tag{4.6}$$

In terms of $\langle M\rangle$, which is the mean number of photoelectrons per integration time per primary aperture, the number of photoelectrons captured by the entire array is $\langle L\rangle = n\langle M\rangle$. Since each main beam is divided into $n-1$ secondary beams, we note that $\langle N\rangle = \langle M\rangle/(n-1)$. Thus Eq. (4.6) simplifies to

$$\mathcal{S}_F = \gamma(n/18)^{1/2}\langle M\rangle^{1/2} = \gamma(\langle L\rangle/18)^{1/2}, \tag{4.7}$$

and using Eq. (4.3) we get

$$\frac{S}{\sigma_S} = \gamma(\langle L\rangle/2)^{1/2}. \tag{4.8}$$

The SNR shown in Eq. (4.8) is identical to that obtained for an ideal Michelson interferometer.[1] Thus we conclude that a ground-based interferometer using the admittedly inferior estimator, the bispectrum phasor, is as good as the ideal Michelson interferometer using directly the fringe phasor, the best estimator, provided that $\gamma^2\langle N\rangle(n-2)^{1/3} \gg 1$. For $n = 6$, for example, by having $\gamma^2\langle N\rangle$ exceed 1/2 one can ensure that one is within 50% of the ideal limit given by Eq. (4.8).

### B. Low Photoelectron Limit

In the low photoelectron limit $[\gamma^2\langle N\rangle(n-2)^{1/2} \ll 1]$ $\mu_b \sim 0$, $\sigma_b \sim \sqrt{8\langle N\rangle^3}$, and

$$\begin{aligned}\mathcal{S}_F &= \left[\frac{n(n-1)(n-2)}{24}\right]^{1/2} \gamma^3\langle N\rangle^{3/2},\\ &= \left[\frac{n(n-2)}{(n-1)(n-1)24}\right]^{1/2} \gamma^3\langle M\rangle^{3/2}.\end{aligned} \tag{4.9}$$

For reasonably large $n$,

$$\frac{S}{\sigma_S} = \sqrt{3/8}\gamma^3\langle M\rangle^{3/2}, \tag{4.10}$$

*independent* of $n$. Thus there is a hard limit to the intensity (since $\langle M\rangle$ is a direct measure of the point-source intensity) of sources that can be imaged with a ground-based ${}^nC_2$ interferometer, and this limit is solely a function of the product of the spatial-coherence area and the temporal-coherence scale set by the atmosphere.

It is easy to understand Eq. (4.10) in terms of the SNR of each of the $n_t$ uncorrelated bispectrum phasors $\mathcal{S}_B$. The SNR in the image must be proportional to $\mathcal{S}_B\sqrt{n_t} \sim \gamma^3(n_t\langle N\rangle^3)^{1/2} \sim \gamma^3\langle M\rangle^{3/2}$, in agreement with Eq. (4.10).

So far we have presented an analysis of the SNR for a point-source model and drawn some conclusions. However, the principal use of bispectral imaging is in obtaining images of extended, noncircular sources. For point sources or binary stars, one can apply much simpler algorithms (which are usually more sensitive as well) rather than use bispectral imaging. Given this, one may question the value of analyses such as the one presented here. In defense of this simplicity we note that the estimation of point-source sensitivity is quite standard in radio astronomy. However, as discussed by one referee, at optical wavelengths the sky is quite dark, and point-source detection is usually not of much interest (however, see below).

Nonetheless, the sensitivity estimate presented here has one principal virtue: it is the best possible performance. The reasoning is as follows. The visibility for a point source is the same on all baselines, long and short. Thus all the baselines will be either in the high photon limit $(\gamma^2\langle N\rangle \gg 1)$ or in the low photon limit. In contrast, for a resolved source $\gamma$ depends on the baseline length and orientation. Since the source is resolved we can safely assume that $\gamma$ is less than unity for all baselines; indeed for most baselines $\gamma$ will be significantly less than unity. With a variable $\gamma$ it is possible that some baselines will be in the low photon limit, in which case the SNR of the bispectrum involving that baseline will be $\propto\gamma^3\langle N\rangle^{3/2}$, considerably worse than for a point source of the same flux density. Thus we expect that the limiting sensitivity for an extended source will be considerably worse than that presented here.

The sensitivity estimates presented here may be optimistic (at the faint end) for another reason as well, because bispectral imaging algorithms are nonlinear by nature and it is possible that these methods fail at low SNR. As an example, Cornwell[12] finds that one particular bispectral method fails when the typical SNR of a bispectrum phasor falls below ~2.5. If this is true of all nonlinear methods then clearly reconstruction of extended objects will be quite affected. These warnings and caveats stress the need for numerical simulations for a true understanding of the limitations of bispectral imaging (in the low photon limit), even for simple sources. However, this is a major exercise in itself, and we will not discuss it in the present paper.

Despite the above pessimistic discussion, there is an important class of astrophysical problems for which point-source detection is the major goal. Specifically, consider optical emission from an active galactic nucleus. Determining the nonthermal contribution from the nuclear region of the host galaxy is of great astrophysical interest. At the high-angular resolution needed for separating the nuclear emission from the host galaxy, long baselines will have to be employed. On such baselines the host galaxy contribution is essentially resolved, leaving only the light from the point source. However, the visibility of the point source is vastly reduced, being equal to the ratio of the nuclear emission to the host-galaxy emission. For this reason, we have permitted $\gamma$ to be less than unity even for a point source. (Additionally, even for a single point source, we expect $\gamma < 1$ for a ground-based interferometer. In this case retaining $\gamma$ in our analysis will give us some idea of the importance of maintaining a high value of $\gamma$.) For both these reasons we will make the less-restrictive assumption $\gamma_j = \gamma$, independent of $j$.

## 5. BISPECTRAL IMAGING AND SELF-CALIBRATION

It is quite instructive and interesting to compare an ${}^nC_2$ radio and an optical interferometer. Clearly, there are fundamental differences: the lack of phase-coherent, low-noise optical amplifiers, heterodyning (versus beam combination), the process of fringe detection, etc. Here we will focus on one aspect: the primary observable and how the atmospheric phase corruption is overcome. Radio arrays usually measure the Michelson fringe phasor and employ the technique of self-calibration in order to get rid of the atmospheric phases, whereas throughout this paper we have assumed that the bispectrum phasor is the primary observable for an ${}^nC_2$ optical interferometer. Given that self-calibration is a mature algorithm (whereas bispectral imaging is not) it is important to explore to what extent self-calibration can be used in the context of an ${}^nC_2$ optical array.

The essence of bispectral imaging is the construction of an image that agrees with the observables (fringe power and bispectrum phases) in a least-squares sense. A number of algorithms have been invented for obtaining images from the bispectral data. In our favorite variant the two primary observables are merged into one quantity, hereafter the synthetic bispectrum phasor, by taking the triple product of the fringe amplitudes $(q_j q_k q_l)^{1/2}$ and by combining this triple product with a unit complex phasor whose phase is the closure phase. This procedure has the advantage that the bispectrum amplitude is better determined since the SNR of the fringe powers is better than that of the bispectrum amplitude, especially at low photon rates. A fit between a model and the data is then obtained by using some kind of least-squares procedure. The details of one such model-fitting algorithm can be found in Ref. 12, and applications to real optical data in Ref. 13.

The basis of self-calibration[14,15] is that the atmospheric phase and gain errors, within one coherent integration interval, can be ascribed to an unknown multiplicative factor that is peculiar to each antenna: $G_j e^{i\theta_j}$, $j = 1, \ldots, n$. A least-squares fit of the current model and the $n$ unknown antenna-based complex gains to the $n_b$ observed complex fringe phasors is done. Constraints on positivity and finiteness are used for making up the shortfall between the number of observables and the number of derived quantities. The entire procedure is iterated until the process converges. According to the simulations performed by Cornwell,[12] self-calibration appears to break down when the SNR of the fringe phasor falls below $\sim$2.5. This is understandable since the complex gains have to be solved from the data itself, and this is possible only if the fringes are readily detected. In Ref. 1 we have shown that the SNR of the fringe phasor is $\alpha \equiv \gamma(\langle N\rangle/2)^{1/2}$. Thus, in our notation, self-calibration is valid for $\alpha \gtrsim 2.5$.

Self-calibration is conceptually simpler than bispectral imaging. In particular, it uses no $n_t(\propto n^3)$ bispectrum phasors but only $n_b(\propto n^2)$ complex fringe phasors. In addition, because it employs *a priori* information (positivity and finite source size), it is quite a powerful algorithm. Finally, there is a large body of self-calibration software developed for radio arrays that has been in use for more than a decade. However, self-calibration does not operate directly on the observable, the bispectrum phasor, and also it does not use all the data since there are $\sim n^3$ bispectrum phasors but only $\sim n^2$ fringe phasors. Clearly, it is important to understand the limitations of both techniques.

First we estimate the sensitivity of the self-calibration technique. As discussed in Subsection 3.A, the fringe phasors are uncorrelated. With $n_b$ fringe phasors and $n$ unknown antenna gains, the number of degrees of freedom is $n_b - n$. The effective signal strength (for a point source) is $(n_b - n)\gamma\langle N\rangle$, and since the image is the Fourier transform of the complex visibility the effective variance is $(n_b - n)\langle N\rangle$. Thus the SNR of the flux density of a point source estimated from a self-calibration map is

$$\left(\frac{S}{\sigma_S}\right)_{SC} = \gamma[(n_b - n)\langle N\rangle]^{1/2} = \alpha[2(n_b - n)]^{1/2}. \tag{5.1}$$

We find that Eq. (5.1) agrees with Eqs. (4.5), which give the SNR of the bispectral-imaging technique, to better than 10% as long as $\alpha \gtrsim 1$, the regime in which self-calibration techniques are used. Thus our immediate conclusion is that for bright sources ($\alpha \gtrsim 1$) there is no difference in sensitivity between bispectral imaging and self-calibration. Hence for such sources the self-calibration software developed for radio interferometers can be immediately applied to an optical ${}^nC_2$ array.

For faint sources ($\alpha \lesssim 1$) it appears that we have no choice but to use the bispectrum observable. In this regime the SNR of the bispectrum $\mathcal{S}_B \sim \gamma^3\langle N\rangle^{3/2}/8 = \alpha^3/2^{3/2}$ is small since $\alpha < 1$. The SNR can be increased by a factor of $\sqrt{N_f}$ by stacking the bispectrum phasors from $N_f$ frames of data. Let us consider a typical example: $\gamma \sim 0.6$ and $N_f \sim 10^4$. Then we find that, in order to have a detectable bispectrum $\mathcal{S}_B \gtrsim 3$ after $N_f$ frames of data, we need to have $\langle N\rangle \gtrsim 0.6$. Increasing $N_f$ by a factor of 10 results in decreasing $\langle N\rangle$ by merely a factor of $\sim$2.

First consider the case for which $n = 3$ so that the beam splitting is minimal. For $\gamma = 0.6$, $\langle N \rangle = 0.6$, we find that $\alpha = 0.33$, and hence $\langle M \rangle = 1.2$. In contrast, the self-calibration limit of $\alpha = 2.5$ corresponds to $\langle M \rangle = 69$. Thus for a ${}^3C_2$ interferometer there is a range in source intensity of a factor of 50 over which we have no choice but to use the bispectrum phasor as the primary observable.

In the more general case, the transition from self-calibration to bispectrum takes place when $\alpha = \gamma(\langle N \rangle/2)^{1/2} = \gamma[\langle M \rangle/2(n-1)]^{1/2}$ falls below $\sim 2$; i.e., the transition takes place when the intensity, $\langle M \rangle$, falls below $8(n-1)\gamma^{-2}$. Thus, superficially, our research indicates that the range of intensity over which the bispectrum phasor will reign supreme is even larger than the above-derived factor of 50 for either arrays with larger elements or when the source starts getting resolved (which decreases $\gamma$). However, we hasten to add that more simulations are needed for pinning down the true threshold above which self-calibration can successfully operate, particularly with complicated source structures and a large number of apertures (see discussion in Section 4).

In sum, for bright sources, existing self-calibration algorithms are certainly adequate for analyzing data from ${}^nC_2$ optical interferometers. For faint sources, we have no recourse but that of using the bispectrum phasor as the primary observable of phase. In this regime, neither self-calibration nor bispectral imaging is optimal. Self-calibration is not optimal because it does not make use of all the $\sim n^3$ bispectrum phasors, which in the low $\alpha$ limit are essentially uncorrelated and hence provide independent estimates of combinations of the fringe phases. Current bispectrum imaging methods are not optimal because they lack a procedure by which reasonable *a priori* assumptions can be introduced into the fitting procedure.

Clearly, a hybrid approach is needed. One possibility is to solve for the Michelson phases by using all the bispectral data and then to use self-calibration for making an image and to iterate, an approach that is already being used at optical wavelengths.[16,17] Another approach is to fit the observed fringe powers and bispectral phases to a model that is subject to the usual conditions of positivity and finite size (as in self-calibration) and to iterate until the model best agrees with the data. We find the second approach pleasing, but we do note that it entails more computing since the number of bispectrum phasors $n_t \sim n^3 \gg n_b \sim n^2$. However, the problem is within the reach of present supercomputers, and we urge the development of this algorithm.

## 6. CONCLUSIONS

We have analyzed the performance of an ${}^nC_2$ optical interferometer, i.e., an interferometer with $n$ apertures in which each primary beam is split into $n-1$ secondary beams that, in turn, are combined two at a time on $n(n-1)/2$ detectors. In this way all the $n(n-1)/2$ spatial frequencies possible with $n$ apertures are simultaneously sampled on separate detectors. An important constraint in optical interferometry with weak signals is that beam splitting must be carried out without the possibility of low-noise, phase-coherent amplifiers.[1] Additionally, as in radio interferometry, aperture-dependent phase errors, such as those caused by atmospheric phase corruption, force us to use the bispectrum phasor, which is an inferior estimator compared with the fringe phasor in an ideal Michelson interferometer.

Owing to the availability of sensitive photoelectric detectors, the primary source of noise in optical interferometry is expected to be that present in the light signal itself, i.e., shot noise of the photoelectric-detection process that obeys Poisson statistics. In contrast, the principal source of noise in radio interferometry is an additive Gaussian noise that primarily arises in the receiving apparatus itself (amplifier noise).

At high enough signal strengths, the fringe phasor and the bispectrum phasor are expected to be equally good estimators, and thus ideal and ground-based imaging interferometers should have similar sensitivities. We find that this expectation is indeed true. Specifically we carry out a rigorous calculation of the SNR of the synthesized image of a point source. We find that the SNR of bispectral imaging approaches that of the ideal Michelson case when $\gamma^2\langle N \rangle (n-2)^{1/2} \gtrsim 1$, where $2\langle N \rangle$ is the number of photons per integration time per detector.

At low photon rates $[\gamma^2\langle N \rangle (n-2)^{1/2} \lesssim 1]$, the SNR in the map is nearly independent of $n$ and depends almost solely on the intensity of the source with a limiting value of $\sqrt{3/8}\gamma^3\langle M \rangle^{3/2}$, where $\langle M \rangle$ is the intensity of the source and is the number of photons per aperture per integration time. This is a result of two compensating factors, as we saw in Section 4, namely, the number of independent bispectrum phasors that grows as $n^3$ and the mean value of each bispectrum phasor that decreases as $n^{-3}$ because of beam splitting. Since the maximum useful area of the aperture can be the spatial coherence area and the maximum integration time the coherence time of the light signal at the apertures, this limiting expression implies that the limiting sensitivity for ground-based optical interferometry is $\langle M \rangle \lesssim 1$. For example, assuming that $\langle M \rangle = 0.3$ and a $\gamma \sim 0.7$ (instrumental decorrelation, etc.), we find that the SNR per frame [Eq. (4.10)] is 0.03. Thus, to get a 5-$\sigma$ detection we would need $1 \times 10^5$ frames, or $\sim$1/2h, assuming a frame integration time of 10 msec. This corresponds to a visual magnitude of 13 (with implicit assumptions of net detective and optical efficiency of 10%, coherence volume, namely, the product of the spatial coherence area and temporal coherence scale, of 0.8 $cm^2$ sec, and a fractional bandwidth of 20%). Insisting that a bispectrum SNR (per frame) be $\gtrsim 2.5$ would result in $\langle M \rangle = 25$ and a limiting magnitude of $\sim 8.5$ (where $n$ is assumed to be 6). These limits are unfortunately somewhat uninteresting in that many of the exciting astrophysical sources, such as active galectic nuclei, are typically a factor of $10^2$ fainter than these limits. This discussion highlights the need for increasing the coherence volume by techniques such as that of the laser guide star.

It is interesting to note that even an ${}^nC_n$ interferometer (i.e., one for which all the $n$ beams combine onto one detector) has the same limiting magnitude[2] as an ${}^nC_2$, up to a factor of order unity. The beam-combination geometry merely changes the intensity at which the transition from an ideal Michelson performance to the less ideal intensity-limited performance occurs.

In the high photon limit, we show that the bispectrum phasors that share a common baseline are correlated with a correlation coefficient of 1/3 and are essentially uncorrelated in the low photon limit. Thus any algorithm designed for producing images from bispectral data must take into account this covariance between the observables.

Since the transition from an ideal Michelson performance to the intensity-limited regime depends on whether $\gamma^2\langle N\rangle(n-2)^{1/2} = \gamma^2\langle M\rangle(n-2)^{1/2}/(n-1) \sim \gamma^2\langle M\rangle n^{-1/2}$ is more than or less than unity, it is clear that the smaller the value of $n$, the better; i.e., the fewer the beam splitters employed, the better it is for sensitivity. This is best seen in Fig. 2 in which we find that there is little gained by going from a 10-element array to a 20-element array. The situation is probably even worse in practice since any systematic error (e.g., stray light due to laser metrology system) will affect a 20-element ${}^nC_2$ array much more than a 10-element array. Thus we argue that it is more efficient to operate a 20-element array as 4 independent 5-element subarrays.

All along we have been restricting our discussion to the point-source sensitivity, whereas in practice interferometers are used for studying a variety of objects. We now argue that beam splitting is deleterious for extended sources as well. The argument has two steps: (1) The transition from the high photon to the low photon regime depends on $\gamma^2\langle M\rangle n^{-1/2}$ being greater than or less than unity, respectively. (2) Once a triplet of baselines is in the low photon regime then the SNR of that bispectrum phasor is very poor: $\gamma^3\langle M\rangle^{3/2}n^{-3/2}$ instead of $\gamma\langle M\rangle^{1/2}n^{-1/2}$. Consider an extended source of a given $\langle M\rangle$. Then those baselines that resolve the source have $\gamma$ considerably below unity. From step (1) it should be clear that with $\gamma$ less than unity it is important to keep $n$ as low as possible in order to keep most baselines in the high photon limit. Thus the smaller the value of $n$, the better it is. Also, as explained in Section 5, it may be that bispectral-imaging methods break down at low SNR's. This agains favors minimizing the beam splitting. From the point of view of image construction, it is necessary to cover as many spatial frequencies as fast as possible. This in turn favors simultaneous measurements of many spatial frequencies, i.e., more beam splitting. However, as was argued in step (2) above, the penalty for being in the low photon limit is severe, and the resulting loss in SNR is not compensated for by the additional increase in the number of baselines (the increase in additional baselines scales as $n^2$, whereas the penalty for a decreased SNR goes as $\gamma^2 n^{-1}$ and for $\gamma \ll 1$ it is easy to see that the trade-off is in favor of small $n$). A compromise is to operate the array as many subarrays with each subarray collecting different sets of spatial frequencies.

In sum, there is a hard limit to the sensitivity of ground-based interferometers $\langle M\rangle \lesssim 1$, independent of $n$. To improve over this limit, we must increase the coherence volume. For compact sources as well as extended sources, we argue that, in the low photon limit, it is better to split the array into multiple subarrays (each measuring either the same set or preferably a different set of spatial frequencies). Use of the subarrays does not improve the limiting sensitivity but improves the dynamic range. This is best realized for compact sources for which the increase is by a factor of $\sqrt{m/n}$, where $m$ is the total number of apertures and $n$ is the number of apertures in one ${}^nC_2$ array. For an extended source the resulting increase in dynamic range is not clear, since, by minimizing beam splitting, we decrease the imaging speed but increase the SNR of the observables. Simulations of extended objects are necessary for obtaining a definitive understanding of this trade-off.

Any instrumental decorrelation, whether due to finite bandwidth, aperture size, source motion, or other reasons, will make the effective photon number smaller by a factor of $\gamma^2$. The limiting SNR in the map also scales as $\gamma^3$. Thus, for the highest sensitivity, instrumental decorrelation should be minimized.

Bispectrum imaging, on account of its insensitivity to the atmospheric phase corruption, can work with low SNR per baseline per frame, while the limiting value of the SNR of the fringe phasor in self-calibration imaging is $\sim$2 per baseline per frame. Thus for bright sources (i.e., the Michelson regime) one need not measure the bispectrum phasors, and self-calibration can be used with the observed Michelson fringe phasors. However, once the SNR of the fringe phasor (per frame) falls below $\sim$2 then the observables that work are the fringe powers and bispectrum phasors. In this regime a large number of frames of data have to be accumulated in order to increase the SNR of the bispectrum phasors. In this limit the bispectrum phasors are uncorrelated, and hence any algorithm should use all the $\sim n^3$ bispectrum phasors. A hybrid algorithm is needed in which, for the first step, the fringe phases are solved for using all the bispectrum data and, in the next step, self-calibration is applied in order to yield an image, etc. Alternatively, following the philosophy of self-calibration, one may attempt iteratively to fit the model directly to the bispectrum phasors by using constraints of positivity and finiteness. We prefer the latter algorithm and urge its development.

## APPENDIX A. SNR OF FRINGE POWER

In this appendix we carry out a rigorous estimate of the fringe power $q_j$. The derivation of variance of fringe power in the case of speckle interferometry can be found in the literature.[7,18] However, these results are not really applicable to an ${}^nC_2$ interferometer employing small apertures (i.e., only one speckle). Our results essentially agree with that of Ref. 7.

Dropping the index $j$ to avoid clutter, we note that

$$
\begin{aligned}
V(q) &= \langle q^2\rangle - \langle q\rangle^2 \\
&= \left\{\sum_p\sum_q \exp[i\omega(p-q)]k(p)k(q) - \sum_r k(r)\right\} \\
&\quad\times\left\{\sum_s\sum_t \exp[-i\omega(s-t)]k(s)k(t) - \sum_u k(u)\right\} \\
&\quad-\left\langle\sum_p\sum_q \exp[i\omega(p-q)]k(p)k(q) - \sum_r k(r)\right\rangle^2 \\
&= \sum_p\sum_q\sum_s\sum_t \exp[i\omega(p-q-s+t)] \\
&\quad\times\langle k(p)k(q)k(s)k(t)\rangle - 2\sum_p\sum_q\sum_u \exp[i\omega(p-q)] \\
&\quad\times\langle k(p)k(q)k(u)\rangle + \sum_r\sum_u \langle k(r)k(u)\rangle \\
&\quad-\left\langle\sum_p\sum_q \exp[i\omega(p-q)]k(p)k(q) - \sum_r k(r)\right\rangle^2,
\end{aligned}
\tag{A1}
$$

where $\omega$ is the spatial frequency corresponding to the baseline $j$. From the general relation in the Poisson statistics for the count $k$ at a given pixel

$$\langle k(k-1)\ldots(k-m+1)\rangle = \langle k\rangle^m, \tag{A2}$$

the following relations for the averages of second-, third-, and fourth-order products of $k(p)$ are obtained:

$$\langle k(p)k(q)\rangle = \langle k(p)\rangle\langle k(q)\rangle + \delta_{pq}\langle k(p)\rangle, \tag{A3}$$

where $\delta_{pq}$ is Kronecker's $\delta$ symbol;

$$\begin{aligned}\langle k(p)k(q)k(r)\rangle &= \langle k(p)\rangle\langle k(q)\rangle\langle k(r)\rangle + \delta_{pq}\langle k(p)\rangle\langle k(r)\rangle \\ &+ \delta_{qr}\langle k(p)\rangle\langle k(q)\rangle + \delta_{rp}\langle k(q)\rangle\langle k(r)\rangle + \delta_{pqr}\langle k(p)\rangle,\end{aligned} \tag{A4}$$

where $\delta_{pqr} = 1(p = q = r)$ or 0 (otherwise); and

$$\begin{aligned}\langle k(p)k(q)k(r)k(s)\rangle &= \langle k(p)\rangle\langle k(q)\rangle\langle k(r)\rangle\langle k(s)\rangle \\ &+ \delta_{pq}\langle k(p)\rangle\langle k(r)\rangle\langle k(s)\rangle + \delta_{pr}\langle k(p)\rangle\langle k(q)\rangle\langle k(s)\rangle \\ &+ \delta_{ps}\langle k(p)\rangle\langle k(q)\rangle\langle k(r)\rangle + \delta_{qr}\langle k(p)\rangle\langle k(q)\rangle\langle k(s)\rangle \\ &+ \delta_{qs}\langle k(p)\rangle\langle k(q)\rangle\langle k(r)\rangle + \delta_{rs}\langle k(p)\rangle\langle k(q)\rangle\langle k(r)\rangle \\ &+ \delta_{pqr}\langle k(p)\rangle\langle k(s)\rangle + \delta_{pqs}\langle k(p)\rangle\langle k(r)\rangle + \delta_{prs}\langle k(p)\rangle\langle k(q)\rangle \\ &+ \delta_{qrs}\langle k(p)\rangle\langle k(q)\rangle + \delta_{pq}\delta_{rs}\langle k(p)\rangle\langle k(r)\rangle \\ &+ \delta_{pr}\delta_{qs}\langle k(p)\rangle\langle k(q)\rangle + \delta_{ps}\delta_{qr}\langle k(p)\rangle\langle k(q)\rangle + \delta_{pqrs}\langle k(p)\rangle,\end{aligned} \tag{A5}$$

where $\delta_{pqrs} = 1(p = q = r = s)$ or 0 (otherwise).

By inserting Eqs. (A3)–(A5) into Eq. (A1), we obtain

$$\begin{aligned}V(q) &= 4\langle N\rangle^2 + 4\langle N\rangle|Z(\omega)|^2 \\ &+ [Z(\omega)^2Z^*(2\omega) + Z^*(\omega)^2Z(2\omega)] + |Z(2\omega)|^2,\end{aligned} \tag{A6}$$

where $Z(\omega) = \sum_{p=0}^{P-1} e^{i\omega p}\langle k(p)\rangle = \gamma_j\langle N\rangle$ and $Z(2\omega) = \sum_{p=0}^{P-1} e^{2i\omega p}\langle k(p)\rangle$. This spurious harmonic noise $Z(2\omega)$ is typical of a photon-noise-limited power spectrum[18] but is completely unimportant for an ${}^nC_2$ array since different baselines correspond to different detectors. Note that terms enclosed in the parentheses correspond to the bispectrum phasor defined by spatial frequencies $\omega$ and $2\omega$. Since each detector has only one spatial frequency, $\omega$, the second harmonic terms are identically zero. We thus finally obtain

$$V(q) = 4\langle N\rangle^2(1 + \gamma_j^2\langle N\rangle). \tag{A7}$$

## ACKNOWLEDGMENTS

Shrinivas R. Kulkarni gratefully acknowledges financial support from the W. M. Keck Foundation. The research of Sudhakar Prasad was supported partially by the Sandia National Laboratories under a Sandia University Research Program contract. Shrinivas R. Kulkarni is a National Science Foundation Presidential Young Investigator and an Alfred P. Sloan Fellow. Tadashi Nakajima holds a Center for Astrophysics Postdoctoral Fellowship. We are grateful to Chris Haniff for several animated discussions on the virtues of self-calculation. We thank Andrea Ghez for a careful reading of the manuscript. We thank the two referees for sharpening up some of the discussion in the paper.

Shrinivas Kulkarni is also with the Owens Valley Radio Observatory, California Institute of Technology. Sudhakar Prasad is also with the Department of Physics and Astronomy, University of New Mexico.

## REFERENCES

1. S. Prasad and S. R. Kulkarni, "Noise in optical synthesis images. I. Ideal Michelson interferometer," J. Opt. Soc. Am. A **6**, 1702–1714 (1989).
2. S. R. Kulkarni, in *JPL Workshop on Space Interferometry*, M. Shao and S. R. Kulkarni, eds. (NASA, Washington, D.C., to be published).
3. M. Born and E. Wolf, *Principles of Optics* (Pergamon, Oxford, 1970), p. 510.
4. T. J. Pearson and A. C. S. Readhead, "Image formation by self-calibration in radio astronomy," Annu. Rev. Astron. Astrophys. **22**, 97–130 (1984).
5. A. R. Thompson, B. G. Clark, C. M. Wade, and P. J. Napier, "The very large array," Astrophys. J. Suppl. Ser. **44**, 151–167 (1980).
6. T. Nakajima and S. R. Kulkarni, "Noise in optical synthesis images. IV. Effects of atmospheric disturbances," submitted to J. Opt. Soc. Am. A.
7. J. C. Dainty and A. H. Greenaway, "Estimation of spatial power spectra in speckle interferometry," J. Opt. Soc. Am. **69**, 786–790 (1979).
8. B. Wirnitzer, "Bispectral analysis at low light levels and astronomical speckle masking," J. Opt. Soc. Am. A **2**, 14–21 (1985).
9. G. R. Ayers, M. J. Northcott, and J. C. Dainty, "Knox–Thompson and triple-correlation imaging through turbulence," J. Opt. Soc. Am. A **5**, 963–985 (1988).
10. T. Nakajima, "Signal-to-noise ratio of the bispectral analysis of speckle interferometry," J. Opt. Soc. Am. A **5**, 1477–1491 (1988).
11. J. W. Goodman, *Statistical Optics* (Wiley, New York, 1985), Chap. 5.
12. T. J. Cornwell, "Radio-interferometric imaging of weak objects in conditions of poor phase stability: the relationship between speckle masking and phase closure methods," Astron. Astrophys. **180**, 269–274 (1987).
13. P. W. Gorham, A. M. Ghez, S. R. Kulkarni, T. Nakajima, G. Neugebauer, J. B. Oke, and T. A. Prince, "Diffraction-limited imaging. III. 30 mas closure phase imaging of six binary stars with the Hale 5 m telescope," Astron. J. **98**, 1783–1799 (1989).
14. T. J. Cornwell and P. N. Wilkinson, "A new method for making maps with unstable radio interferometers," Mon. Not. R. Astron. Soc. **196**, 1067–1086 (1981).
15. F. R. Schwab, "Adaptive calibration of radio interferometer data," in *1980 International Optical Computing Conference (Book I)*, W. T. Rhodes, ed., Proc. Soc. Photo-Opt. Instrum. Eng. **231**, 18–25 (1980).
16. C. A. Haniff, C. D. Mackay, D. J. Titterington, D. Sivia, and P. J. Warner, "The first images from optical aperture synthesis," Nature (London) **328**, 694–696 (1987).
17. T. Nakajima, S. R. Kulkarni, P. W. Gorham, A. M. Ghez, G. Neugebauer, J. B. Oke, T. A. Prince, and A. C. S. Readhead, "Diffraction-limited imaging. II. Optical aperture-synthesis imaging of two binary stars," Astron. J. **97**, 1510–1521 (1989).
18. J. W. Goodman and J. F. Belsher, "Photon limited images and their restoration," Tech. Rep. RADC-TR-76-50 (Rome Air Development Center, New York, 1976); "Precompensation and postcompensation of photon limited degraded images," Tech. Rep. RADC-TR-77-175 (Rome Air Development Center, New York, 1977).